UMYU Scientifica, Vol. 5 NO. 2, June 2026, Pp 265 – 283
https://doi.org/10.56919/usci.2652.025
ISSN: 2955 – 1145 (print); 2955 – 1153 (online)
A periodical of the Faculty of Natural and Applied Sciences, UMYU, Katsina

ORIGINAL RESEARCH ARTICLE

A Deterministic Model of Cholera Transmission with Vaccination, Environmental Reservoirs, and Vector Dynamics

Abdullahi Ahmed[1,2,3], Adamu Ishaku[2,3], Ahmadu Bappah Muhammad[2,3] and Ayuba Sanda[2,3]
[1]Department of Mathematics and Computer Science, College of Education Billiri, Gombe, Nigeria
[2]Department of Mathematical Sciences, Gombe State University, Gombe, Nigeria
[3]GSU-Mathematics for Innovative Research (GSU-MIR) Group, Department of Mathematics, Gombe State University, Gombe, Nigeria

ABSTRACT
This research develops an extended deterministic model to investigate the transmission dynamics of cholera by incorporating three critical components: vaccinated human population, an exposed human compartment, and vector recruitment, which was modelled using logistic growth that contributes to environmental contamination. The model was analyzed by examining the stability of its equilibrium points. The analysis shows that the basic reproduction number, R_0, controls disease dynamics. It is shown that the disease-free equilibrium is locally asymptotically stable when $R_0 < 1$ and unstable when $R_0 > 1$, leading to endemic persistence. In an attempt to examine the effect of some parameters on disease dynamic, parameter estimation was performed using available epidemiological data, and model validation was conducted using root mean square error (RMSE) and coefficient of determination (R^2); sensitivity analysis was employed using Partial Rank Correlation Coefficients (PRCC), revealing that transmission rates and environmental contamination parameters significantly influence disease spread. Finally, numerical simulations are also performed to verify the analytic results. Analytical results show that the combined effects of vaccination coverage, environmental contamination, and vector density strongly influence cholera transmission. Although increasing vaccination reduces transmission, the presence of reinfection and environmental reservoirs may sustain the disease even when the reproduction number is close to unity. Numerical simulations are performed to support the theoretical findings and to illustrate the impact of key parameters on disease dynamics. Generally, this research highlights the importance of integrating control strategies, including vaccination, access to clean water, proper sanitation, vector control, and early treatment, to achieve effective and sustainable cholera control in endemic settings.

ARTICLE HISTORY
Received January 29, 2026
Accepted May 24, 2026
Published June 18, 2026

KEYWORDS
Cholera; Mathematical modelling; Stability analysis; Sensitivity analysis; Numerical simulations.

INTRODUCTION
Cholera is a short-term, life-threatening disease caused by the bacterium *Vibrio cholerae*. The disease affects the intestine and causes diarrhoea (WHO, 2011). Cholera exists in different serogroups, but the serogroups responsible for outbreaks are 01-0139 (CDC, 2019). Diarrhea the main symptom of cholera and is often referred to as acute diarrheal disease. It is accompanied by severe dehydration, which can lead to death within hours if not treated. The disease remains asymptomatic for 12 hours to 5 days after ingestion of contaminated food or water. Nonetheless, infected individuals may still shed the bacterium, contaminating the environment and posing risks to others (WHO, 2011). Cholera is primarily transmitted through ingestion of food or water contaminated with *V. cholerae*, making unhygienic environments highly vulnerable to outbreaks.

Furthermore, direct human-to-human contact, such as handshakes, can facilitate transmission (Yang et al., 2017). People with low immunity, such as malnourished children or people living with HIV, have a higher tendency to develop cholera (Hove-Musekwa et al., 2011). To prevent the spread of cholera, proper environmental sanitation is necessary, along with access to clean water and safe food. Vaccination also plays a significant role in reducing the prevalence of the disease (WHO, 2011). Treatment primarily (CDC, 2019) involves rapid replacement of lost fluids and salts using oral rehydration solutions (ORS) (WHO, 2011).

Correspondence: Abdullahi Ahmed. Department of Mathematics and Computer Science, College of Education Billiri, Gombe, Nigeria. ✉ abdulahmedyauta@gmail.com.
How to cite: Ahmed, A., Ishaku, A., Bappah, A. M., & Sanda, A. (2026). A Deterministic Model of Cholera Transmission with Vaccination, Environmental Reservoirs, and Vector Dynamics. *UMYU Scientifica*, 5(2), 265 – 283. https://doi.org/10.56919/usci.2652.025

Individuals who recover from cholera acquire immunity that can protect them for many years (Harris et al., 2012).

Globally, between 1.3 and 4.0 million cases are estimated and 21,000 to 143,000 deaths from cholera each year (WHO, 2011). The current pandemic began in 1961 in Indonesia and spread to Europe, the South Pacific and Japan by the late 1970s and to South America by the 1990s. Notable outbreaks have occurred in India (2007), Congo, Zimbabwe, and Iraq (2008), Vietnam and Zimbabwe (2009), and Nigeria and Haiti (2010). In Nigeria, cholera is a recurring disease that often peaks during the rainy season. Major epidemics were recorded in 1970, 1990, and between 1992–1997. In 2010, the Federal Ministry of Health reported 37,289 cases and 1,434 deaths between January and October. In 2011, there were 22,797 cases and 728 deaths. The Nigeria Centre for Disease Control (NCDC) reported 42,466 suspected cases and 830 deaths in 2018 (CDC, 2019). In 2021, cholera led to 103,589 infections and 3,566 deaths—surpassing the COVID-19 death toll of 2,977 in the same year (CDC, 2021). As of August 11, 2024, a total of 5,951 suspected cholera cases and 176 deaths had been reported across Nigeria's 36 states (CDC, 2024). Cholera is a food-borne enteric disease caused by the bacterium *Vibrio cholerae*. Globally, it accounts for an estimated 1.6% to 3.5% of food-borne disease-related deaths and 1.3 to 4.0 million cases annually In developing countries, food-borne diseases like cholera remain prevalent due to poor hygiene, lack of education, inadequate drainage systems, and the abundance of carriers (Misra et al., 2013). Promoting awareness about safe food storage and enhancing environmental sanitation can reduce the incidence of food-borne diseases (Lata et al., 2020). These diseases are also transmitted by vectors such as houseflies, ticks, and mites. Houseflies, in particular, are known mechanical vectors for various pathogens, including bacteria (Levine & Levine, 1991). Studies suggest that houseflies contribute significantly to cholera transmission (Keiding, 1986), especially during seasons of high fly density (Levine & Levine, 1991). Although humans rarely interact directly with houseflies, the fly population in the environment still significantly influences cholera transmission dynamics (Lata et al., 2020). Studies estimate that infected vectors can shed approximately 1,000 vibrios per gram of stool for 1 day (Nelson et al., 2009). Therefore, vectors such as houseflies play a crucial role in the transmission of cholera.

Several mathematical models have been developed to study cholera transmission (Fister et al., 2016). A common model structure is the SIRB framework, which incorporates bacterial concentration in contaminated water as an environmental class alongside human compart-ments. Extensions of the SIRB model include asymptomatic infectious compartments and hyper-infectious bacteria classes (Das et al., 2005), while others include partial immunity and person-to-person transmission (Pascual et al., 2006). Another study (Edward & Nyerere, 2015) explored the impact of vaccination, treatment, sanitation, and awareness campaigns on cholera control. While many models focus on direct human-to-human transmission and indirect transmission via contaminated water, fewer studies have addressed the role of vectors in cholera spread such as (Kaka & Anteneh, 2024; Lata et al., 2020; Al-Shanfari et al., 2019; Omondi, 2016; Fotedar et al., 1992; Levine & Levine, 1991). Vectors are increasingly recognized as major contributors to the global transmission of cholera, especially in developing countries (Das et al., 2005). A model proposed in (Kaka & Anteneh, 2024) introduced a compartmental framework involving human hosts, vectors, and environmental reservoirs. However, the model did not consider vaccination and exposure compartments for humans. In this study, we extend the model in (Kaka & Anteneh, 2024) by incorporating a vaccinated class and an exposed human compartment. We also model vector recruitment using a logistic growth function rather than a constant rate to provide a more realistic representation. C ontaminated and uncontaminated zones remains. The inclusion of the exposed human class targets the model's realism, capturing the latent period before individuals become infectious and helping to better understand cholera transmission dynamics.

MODEL FORMULATION

The model (Figure 1) considers two host populations: human and vector populations. It incorporates both direct and indirect environmental transmission by modeling the dynamics of free-living Vibrio cholerae concentrations in safe and unsafe environments. The human population is divided into five compartments: Susceptible individuals $S_h(t)$, Vaccinated individuals $V_h(t)$, Exposed individuals $E_h(t)$, Infected individuals $I_h(t)$, Recovered individuals $R_h(t)$. Susceptible individuals are vaccinated at a constant rate ω, while vaccine protection wanes at rate ψ. The environmental bacterial concentrations are denoted by P(t) (safe environment) and $C(t)$ (unsafe environment). We define: β_1: Environment-to-human transmission rate β_2: Human-to-human transmission rate k: Half-saturation constant of the bacterial concentration. The force of infection for humans is defined by:

$$\lambda_h = \frac{\beta_1 P}{k + P} + \beta_2 I_h \tag{1}$$

The vector population in the model is divided into two compartments: susceptible vectors $S_v(t)$, and exposed vectors $E_v(t)$. In this population, exposure occurs when susceptible vectors come into contact with infected human faeces in an unsafe environment C(t) or with a previously safe environment P(t) that has been contaminated. The rate at which susceptible vectors are exposed, denoted by λ_v, is modeled as a nonlinear function that incorporates saturation effects:

$$\lambda_v = \frac{\tau_1 C}{k_1 + C} + \frac{\tau_2 P}{k_2 + P} \quad (2)$$

Here, τ_1 and τ_2 represent the contact rates with unsafe and safe environments, respectively, while k_1 and k_2 are the corresponding half-saturation constants.

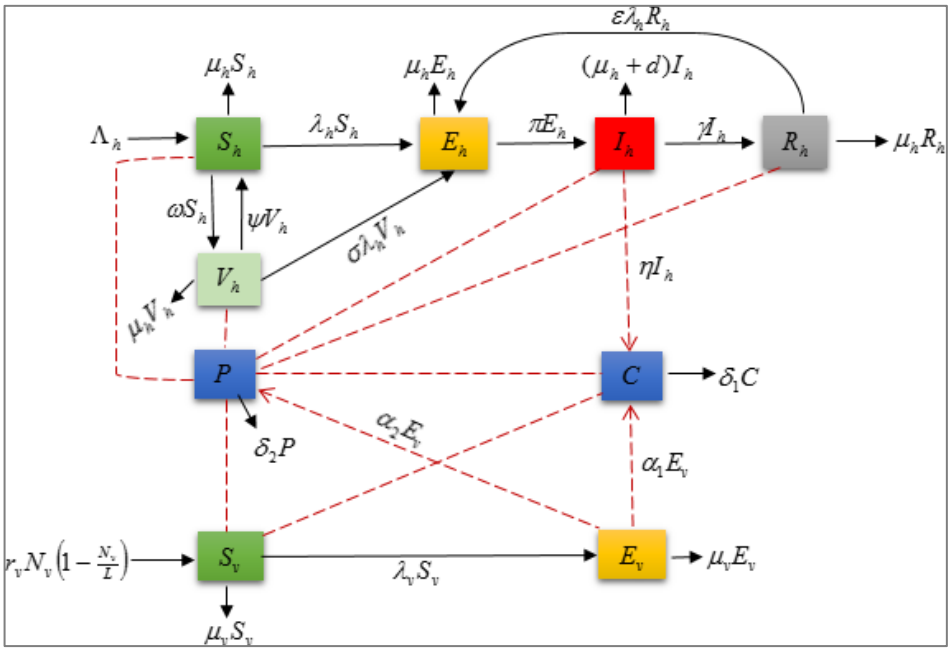

Figure 1: Model Diagram

The model equation is given by

$$\begin{aligned}
\frac{dS_h}{dt} &= \Lambda_h - \lambda_h S_h - (\mu_h + \omega)S_h + \psi V_h \\
\frac{dE_h}{dt} &= \lambda_h S_h + \sigma\lambda_h V_h + \varepsilon\lambda_h R_h - (\mu_h + \pi_h)E_h \\
\frac{dV_h}{dt} &= \omega S_h - (\mu_h + \psi)V_h - \sigma\hat{\lambda}_h V_h \\
\frac{dI_h}{dt} &= \pi_h E_h - (\mu_h + d + \gamma)I_h \\
\frac{dR_h}{dt} &= \gamma I_h - \mu_h R_h \\
\frac{dS_v}{dt} &= r_v N_v\left(1 - \frac{N_v}{L}\right) - \lambda_v S_v - \mu_v S_v \\
\frac{dE_v}{dt} &= \lambda_v S_v - \mu_v E_v \\
\frac{dC}{dt} &= \eta I_h + \alpha_1 E_v - \delta_1 C \\
\frac{dP}{dt} &= \alpha_2 E_v - \delta_2 P
\end{aligned} \quad (3)$$

with initial conditions

$$S_h(0) > 0, E_h(0) \geq 0, V_h(0) \geq 0, I_h(0) \geq 0, R_h(0), S_v(0) > 0, E_v(0) \geq 0, C(0) \geq 0, P(0) \geq 0$$

Basic Properties of the Model

Positivity of Solutions

The model (3) monitors a population that cannot be negative; thus, we verify the positivity of the solutions to the model system (3), assuming non-negative initial conditions. This step confirms that the populations and concentrations involved do not attain negative values at any time $t \geq 0$. Let ($S_h = x_1$, $E_h = x_2$, $V_h = x_3$, $I_h = x_4$, $R_h = x_5$, $S_v = x_6$, $E_v = x_7$, $C = x_8$, $P = x_9$) in system of equations (3), we get

$$\begin{aligned}
\frac{dx_1}{dt} &= \Lambda_h - \left(\frac{\beta\, x_9}{k + x_9} + \beta_2 x_4\right)x_1 - (\mu_h + \omega)x_1 + \psi x_3 \\
\frac{dx_2}{dt} &= \left(\frac{\beta\, x_9}{k + x_9} + \beta_2 x_4\right)x_1 + \sigma\left(\frac{\beta\, x_9}{k + x_9} + \beta_2 x_4\right)x_3 + \varepsilon\left(\frac{\beta\, x_9}{k + x_9} + \beta_2 x_4\right)R_h - (\mu_h + \pi_h)E_h \\
\frac{dx_3}{dt} &= \omega x_1 - (\mu_h + \psi)x_3 - \sigma\left(\frac{\beta\, x_9}{k + x_9} + \beta_2 x_4\right)x_3 \\
\frac{dx_4}{dt} &= \pi_h x_2 - (\mu_h + d + \gamma)x_4 \\
\frac{dx_5}{dt} &= \gamma x_4 - \varepsilon\left(\frac{\beta\, x_9}{k + x_9} + \beta_2 x_4\right)x_5 - \mu_h x_5 \\
\frac{dS_v}{dt} &= r_v(x_6 + x_7)\left(1 - \frac{(x_6 + x_7)}{L}\right) - \left(\frac{\tau_1 x_8}{k_1 + x_8} + \frac{\tau_2 x_9}{k_2 + x_9}\right)x_6 - \mu_v x_6 \\
\frac{dx_7}{dt} &= \left(\frac{\tau_1 x_8}{k_1 + x_8} + \frac{\tau_2 x_9}{k_2 + x_9}\right)x_6 - \mu_v x_7 \\
\frac{dx_8}{dt} &= \eta x_4 + \alpha_1 x_7 - \delta_1 x_8 \\
\frac{dx_9}{dt} &= \alpha_2 x_7 - \delta_2 x_9
\end{aligned} \tag{4}$$

with initial conditions

$x_i(0) \geq 0 \qquad i = 1, 2, \ldots, 9$

Lemma 3.1. If the initial conditions satisfy $x_i(0) \geq 0$ for all $i = 1, 2, \ldots, 9$, then the corresponding solutions $x_i(t)$, for $i = 1, 2, \ldots, 9$, remain positive for all $t \geq 0$.

Proof. We prove the lemma by contradiction, following the method used to establish the positivity of solutions in systems of nonlinear equations, as discussed in (Ishaku & Hussaini, 2020; Hai-Feng & Na-Na, 2012).

Suppose, contrary to the claim, that there exists a time t_j such that

$$x_j(t_j) = 0, \frac{dx_j(t_j)}{dt} < 0, \qquad \text{for some } j = 1,2,3,\ldots,9 \tag{5}$$

$$x_i(t) > 0 \quad \text{for } i \neq j, \quad i = 1,2,3,\ldots,9, \quad \text{for } 0 < t < t_j \tag{6}$$

Since all the parameters of the model are positive, we evaluate $x'(t_j)$ for each j under equation

(5), using the system of equations in model (3):

For $j = 1$ then $x_1 = 0$, $\qquad \frac{dx_1(t_1)}{dt} = \Lambda_h + \psi x_3 > 0$ (7)

For $j = 2$ then $x_2 = 0$,

$$\frac{dx_2(t_2)}{dt} = \left(\frac{\beta\, x_9}{k + x_9} + \beta_2 x_4\right)x_1 + \sigma\left(\frac{\beta\, x_9}{k + x_9} + \beta_2 x_4\right)x_3 + \varepsilon\left(\frac{\beta\, x_9}{k + x_9} + \beta_2 x_4\right)x_5 > 0 \quad (8)$$

For $j = 3$ then $x_3 = 0$, $\quad \frac{dx_3(t_3)}{dt} = \omega x_1 > 0$ (9)

For $j = 6$ then $x_6 = 0$, $\quad \frac{dx_6(t_6)}{dt} = r_v x_7\left(1 - \frac{x_7}{L}\right) > 0$ (10)

For $j = 7$ then $x_7 = 0$, $\quad \frac{dx_7(t_7)}{dt} = \left(\frac{\tau_1 x_8}{k_1 + x_8} + \frac{\tau_2 x_9}{k_2 + x_9}\right)x_6 > 0$ (11)

Similarly, one can show that $x'(t_j) > 0$ for $j = 3, 4, 5, 6, 7, 8, 9$, using the fact that $x_i(t) > 0$ for $i \neq j$ and all parameters are positive.

This contradicts the assumption that $x_j(t_j) = 0$ and $x'(t_j) < 0$, since we have shown that

$x'(t_j) \geq 0$ in all cases.

Therefore, the assumption must be false, and the solution satisfies

$x_i(t) > 0$ for all $i = 1, 2, 3, \ldots, 9$, and $t \geq 0$.

Invariant Region

Theorem 3.1. the close set $\Omega_h = \left\{(S_h, E_h, V_h, I_h, R_h,) \in \Re_+^5 : N_h \leq \frac{\Lambda_h}{\mu_h}\right\}$ and $\Omega_v = \left\{(S_v, E,) \in \Re_+^2 : N_v \leq L\right\}$

are positively invariant and attracting with respect to the model (3). The biologically feasible region is given by the set $\Omega = \Omega_h \times \Omega_V$.

Proof. Adding the equations in model (3) where $N_h = S_h + V_h + E_h + I_h + R_h$, $\quad N_v = S_v + E_v$

denote the total human and vector populations, respectively.

$$\Omega_h = \left\{(S_h, E_h, V_h, I_h, R_h,) \in \Re_+^5 : N_h \leq \frac{\Lambda_h}{\mu_h}\right\}$$

$$\frac{dN}{dt} = \Lambda_h - \mu_h N_h - dI_h$$

Since all the model parameters are positive for all $t > 0$, then the following inequality holds,

$$\frac{dN}{dt} \leq \Lambda_h - \mu_h N_h \quad (12)$$

$$\frac{dN}{dt} + \mu_h N_h \leq \Lambda_h \quad (13)$$

Solving the above differential inequality using the integrating factor procedure, we get

$$u(t) = e^{\int \mu_h dt} = e^{\mu_h t} \quad (14)$$

So, the solution becomes

As $t \to \infty$ $\lim_{t\to\infty} \sup N_h(t) \le \frac{\Lambda_h}{\mu_h}$ (15)

Thus, the total human population $N_h(t)$ is bounded above by $\frac{\Lambda_h}{\mu_h}$ as $t \to \infty$. Further, $N_h(t) \le \frac{\Lambda_h}{\mu_h}$

Thus, Ω is positively invariant.

For Vector population

$$\Omega_v = \left\{(S_v, E,) \in \Re_+^2 : N_v \le L\right\} \quad (16)$$

solving the logistic growth equation for vector population

$$\frac{dN_v}{dt} = r_v N_v\left(1 - \frac{N_v}{L}\right) - \mu_h N_v \quad (17)$$

Let $y = N_v$ solving the logistic equation

$$\frac{dy}{dt} \le r_v y\left(1 - \frac{y}{L}\right) \quad (18)$$

Using Variable separable

$$\frac{1}{y\left(1 - \frac{y}{L}\right)} dy \le r_v dt \quad (19)$$

Putting $y(t) = N(t)$

$$N_v(t) \le \frac{LC_1 e^{rt}}{1 + C_1 e^{rt}} = \frac{L}{1 + \left(\frac{L - y_0}{N_0}\right)e^{-rt}} \quad (20)$$

As $t \to \infty$

$$\lim_{t\to\infty} \sup N_v(t) \le \frac{L}{1+0} = L \quad (21)$$

Thus, the total vector population $N_v(t)$ is bounded above by L (carrying capacity) as $t \to \infty$.
Further, $N_v(t) \le L$. Thus, Ω is positively invariant.
However, for the pathogen, the boundedness is shown as follows:

$$\frac{dC}{dt} = \eta I_h + \alpha_1 E_v - \delta_1 C \quad (22)$$

But

$$I_h \le \frac{\Lambda_h}{\mu_h}, \quad E_v \le L$$

Then

$$\frac{dC}{dt} \le \eta \frac{\Lambda_h}{\mu_h} + \alpha_1 L - \delta_1 C \tag{23}$$

By integrating this inequality using the integrating factor $I.F = e^{\delta_1 t}$, the solution becomes

$$C(t) \le \frac{\eta \Lambda_h}{\delta_1 \mu_h} + \frac{\alpha_1}{\delta_1} L + A e^{-\delta_1 t} \tag{24}$$

Where a is a constant, then

$$\lim_{t \to \infty} \; C(t) \le \frac{\eta \Lambda_h}{\delta_1 \mu_h} + \frac{\alpha_1}{\delta_1} L \tag{25}$$

By integrating this inequality using the integrating factor $I.F = e^{\delta_2 t}$, the solution becomes

$$P(t) \le \frac{\alpha_2}{\delta_2} L + A e^{-\delta_2 t} \tag{26}$$

Where A is a constant, then

$$\lim_{t \to \infty} \; P(t) \le \frac{\alpha_2}{\delta_2} L \tag{27}$$

Hence

$$0 \le N_h(t) \le \frac{\Lambda_h}{\mu_h}, \quad 0 \le N_v(t) \le L, \quad 0 \le C(t) \le \frac{\eta \Lambda_h}{\delta_1 \mu_h} + \frac{\alpha_1}{\delta_1} L, \quad 0 \le P(t) \le + \frac{\alpha_2}{\delta_2} L$$

which implies that N_h, N_v, and all other variables (S_h, V_h, E_h, I_h, R_h, S_v, E_v, C, P) of model equations (3) are bounded and all the solutions starting in Ω approach, enter, or stay in Ω. Hence, the set Ω is positively invariant, that is, all the solutions in Ω remain in Ω for $t \ge 0$.

Disease-Free Equilibrium

The Disease-Free Equilibrium (DFE) of the cholera model is a steady-state in which no infection exists in the population or the environment. It is defined by setting the right- hand side of system (3) to zero;

Thus, the disease-free equilibrium of the model is

$$E_0 = \left(S_h^0, E_h^0, V_h^0, I_h^0, R_h^0, S_v^0, E_v^0, C^0, P^0 \right)$$

$$E_0 = \left(\frac{\Lambda_h(\mu_h + \psi)}{\mu_h(\mu_h + \omega + \psi)}, 0, \frac{\omega \Lambda_h}{\mu_h(\mu_h + \omega + \psi)}, 0, \; 0, L\left(1 - \frac{\mu_h}{r_v}\right), 0, 0, 0 \right) \tag{28}$$

Basic Reproduction Number

In epidemiology, a key threshold known as the basic reproduction number is defined as the average number of secondary infectious cases generated by a single primary infectious case introduced into an entirely susceptible population. To compute R_0, we use the next-generation matrix approach described in (van den Driessche & Watmough, 2002), where R_0 is obtained as the largest eigenvalue (spectral radius) of the matrix

$$R_0 = \rho\left(FV^{-1}\right) \tag{29}$$

Evaluating both F and V by taking the partial derivatives of the terms in F and V at the disease free equilibrium we have.

$$F = \begin{bmatrix} 0 & (S_h^0+\sigma V_h^0)\beta_2 & 0 & 0 & (S_h^0+\sigma V_h^0)\frac{\beta_1}{k} \\ 0 & 0 & 0 & 0 & 0 \\ 0 & 0 & 0 & S_v^0\frac{\tau_1}{k_1} & S_v^0\frac{\tau_2}{k_2} \\ 0 & 0 & 0 & 0 & 0 \\ 0 & 0 & 0 & 0 & 0 \end{bmatrix}, \quad V = \begin{bmatrix} a_1 & 0 & 0 & 0 & 0 \\ \pi_h & a_2 & 0 & 0 & 0 \\ 0 & 0 & \mu_v & 0 & 0 \\ 0 & -\eta & -\alpha_1 & \delta_1 & 0 \\ 0 & 0 & -\alpha_2 & 0 & \delta_2 \end{bmatrix} \tag{30}$$

Where

$$a_1 = \mu_h + \pi_h, \quad a_2 = \mu_h + d + \gamma \tag{31}$$

$$S_h^0 = \frac{\Lambda_h(\mu_h+\psi)}{\mu_h(\mu_h+\psi+\omega)}, \quad S_v^0 = L\left(1-\frac{\mu_v}{r_v}\right) \tag{32}$$

Thus

$$FV^{-1} = \begin{bmatrix} \frac{\beta_2(S_h^0+\sigma V_h^0)}{a_1a_2} & \frac{\beta_2(S_h^0+\sigma V_h^0)}{a_2} & \frac{\beta_2(S_h^0+\sigma V_h^0)}{\delta_2k\mu_2} & 0 & \frac{\beta_2(S_h^0+\sigma V_h^0)}{\delta_2k} \\ 0 & 0 & 0 & 0 & 0 \\ \frac{S_v^0\eta\pi_h\tau_1}{a_1a_2\delta_1k_1} & \frac{S_v^0\eta\tau_1}{a_2\delta_1k_1} & \frac{S_v^0\alpha_1\tau_1}{\delta_1k_1\mu_v}+\frac{S_v^0\alpha_2\tau_2}{\delta_2k_2\mu_v} & \frac{S_v^0\tau_1}{\delta_1k_1} & \frac{S_v^0\tau_2}{\delta_2k_2} \\ 0 & 0 & 0 & 0 & 0 \\ 0 & 0 & 0 & 0 & 0 \end{bmatrix} \tag{33}$$

The characteristic polynomial of FV^{-1} result to

$$\lambda^2(\lambda^2 - (A+D)\lambda + (AD-BC)) = 0 \tag{34}$$

Which gives

$$\lambda_1 = 0, \quad \lambda_2 = 0, \quad \lambda^2 - (A+D)\lambda + (AD-BC) = 0$$

$$R_0 = \rho\left(FV^{-1}\right) = \frac{1}{2}\left((A+D) + \sqrt{(A-D)^2+4BC}\right) \tag{35}$$

Where

$$A = \frac{\beta_2\pi_h\Lambda_h\left[(\mu_h+\psi)+\sigma\omega\right]}{a_1a_2\mu_h(\mu_h+\omega+\psi)}, \quad B = \frac{\beta_1\Lambda_h\left[(\mu_h+\psi)+\sigma\omega\right]}{\delta_2k\mu_v\mu_h(\mu_h+\omega+\psi)}, \quad C = \frac{L\left(1-\frac{\mu_v}{r_v}\right)\eta\pi_h\tau_1}{a_1a_2\delta_1k_1}, \quad D = \frac{L\left(1-\frac{\mu_v}{r_v}\right)\alpha_1\tau_1}{a_1k_1\mu_v} + \frac{L\left(1-\frac{\mu_v}{r_v}\right)\alpha_2\tau_2}{\delta_2k_2\mu_v} \tag{36}$$

Following the theorem of van den Driessche & Watmough (2002), we state the following result.

Theorem 5.1. The disease-free equilibrium E_0 of the cholera model (3) is locally asymptotically stable if $R_0 < 1$ and unstable if $R_0 > 1$.

The DFE strongly influences the behavior of disease transmission dynamics in the population. This implies that if we are looking to eliminate cholera from the population, we have to establish the conditions necessary for the cholera-free equilibrium to be stable. Epistemologically, when R0 < 1, on average each infected individual infects fewer than 1 individual, and the disease dies out. On the other hand, if $R_0 > 1$, each infected individual, on average, infects more than one other individual, and we would expect the disease to spread. However, this depends on the initial sizes of infected persons.

Backward Bifurcation

The significance of examining backward bifurcation is that the classical requirement of $R_0 < 1$ is necessary but not sufficient for effective disease elimination. Consequently, the dynamics of cholera transmission with backward bifurcation are difficult to control. This phenomenon has been reported in several epidemiological contexts; see, for example, (Ishaku and Hussain 2024). Therefore, it is always important to examine the possibility of backward bifurcation before exploring the global stability. We then examine the presence of backward bifurcation in accordance with (Ishaku & Hussaini, 2020) by applying Center Manifold theory. The outcome is shown as follows: let $S_h = x_1$, $E_h = x_2$, $V_h = x_3$, $I_h = x_4$, $R_h = x_5$, $S_v = x_6$, $E_v = x_7$, $C = x_8$, $P = x_9$ and the total population is given by $N = x_1 + x_2 + x_3 + x_4 + x_5 + x_6 + x_7 + x_8 + x_9$ Furthermore, using the vector representation $X = (x_1, x_2, x_3, x_4, x_5, x_6, x_7, x_8, x_9)$, the cholera dynamical system (3) will be re-written as

$$\frac{dX}{dt} = Y(X) \tag{37}$$

$$\begin{aligned}
\frac{dx_1}{dt} &= \Lambda_h - \left(\frac{\beta\, x_9}{k + x_9} + \beta_2 x_4\right)x_1 - (\mu_h + \omega)x_1 + \psi x_3 \\
\frac{dx_2}{dt} &= \left(\frac{\beta\, x_9}{k + x_9} + \beta_2 x_4\right)x_1 + \sigma\left(\frac{\beta\, x_9}{k + x_9} + \beta_2 x_4\right)x_3 + \varepsilon\left(\frac{\beta\, x_9}{k + x_9} + \beta_2 x_4\right)R_h - (\mu_h + \pi_h)E_h \\
\frac{dx_3}{dt} &= \omega x_1 - (\mu_h + \psi)x_3 - \sigma\left(\frac{\beta\, x_9}{k + x_9} + \beta_2 x_4\right)x_3 \\
\frac{dx_4}{dt} &= \pi_h x_2 - (\mu_h + d + \gamma)x_4 \\
\frac{dx_5}{dt} &= \gamma x_4 - \varepsilon\left(\frac{\beta\, x_9}{k + x_9} + \beta_2 x_4\right)x_5 - \mu_h x_5 \\
\frac{dS_v}{dt} &= r_v(x_6 + x_7)\left(1 - \frac{(x_6 + x_7)}{L}\right) - \left(\frac{\tau_1 x_8}{k_1 + x_8} + \frac{\tau_2 x_9}{k_2 + x_9}\right)x_6 - \mu_v x_6 \\
\frac{dx_7}{dt} &= \left(\frac{\tau_1 x_8}{k_1 + x_8} + \frac{\tau_2 x_9}{k_2 + x_9}\right)x_6 - \mu_v x_7 \\
\frac{dx_8}{dt} &= \eta x_4 + \alpha_1 x_7 - \delta_1 x_8 \\
\frac{dx_9}{dt} &= \alpha_2 x_7 - \delta_2 x_9
\end{aligned} \tag{38}$$

Where

$$N_v = x_6 + x_7$$

$$\lambda_h = \frac{\beta_1 x_9}{k + x_9} + \beta_2 x_4$$

$$\lambda_v = \frac{\tau_1 x_8}{k_1 + x_8} + \frac{\tau_2 x_9}{k_2 + x_9} \quad ,$$

consider the case when $R_0 = 1$. Suppose, that β_2 is chosen as a bifurcation parameter, implies $\beta_2 = \beta^*$ Given a system of ODEs The Jacobian matrix is defined as

$$J(x)=\begin{pmatrix} -\lambda-(\mu_h+\psi) & 0 & \psi & -x_1\beta_2 & 0 & 0 & 0 & 0 & -x_1\beta_1\frac{k}{(k+x_9)^2} \\ \lambda_h & -(\mu_h+\pi_h) & \sigma\lambda_h & \beta_2(x_1+\varpi x_3+\varepsilon x_5) & \varepsilon\lambda_h & 0 & 0 & 0 & \beta_1\frac{k}{(k+x_9)^2}(x_1+\varpi x_3+\varepsilon x_5) \\ \omega & 0 & -(\mu_h+\psi)-\sigma\lambda_h & -\varpi x_3\beta_2 & 0 & 0 & 0 & 0 & -\varpi x_3\beta_1\frac{k}{(k+x_9)^2} \\ 0 & \pi_h & 0 & -(\mu_h+d+\gamma) & 0 & 0 & 0 & 0 & 0 \\ 0 & 0 & 0 & \gamma-\varepsilon x_5\beta_2 & -(\varepsilon\lambda_h+\mu_h) & 0 & 0 & 0 & -\varepsilon x_5\beta_1\frac{k}{(k+x_9)^2} \\ 0 & 0 & 0 & 0 & 0 & r_v(1-\frac{2N_v}{L})-\lambda_v-\mu_v & r_v(1-\frac{2N_v}{L}) & -x_6\tau_1\frac{k_1}{(k+x_9)^2} & -x_6\tau_2\frac{k_2}{(k+x_9)^2} \\ 0 & 0 & 0 & 0 & 0 & \lambda_v & -\mu_h & -x_6\tau_1\frac{k_1}{(k+x_9)^2} & x_6\tau_2\frac{k_2}{(k+x_9)^2} \\ 0 & 0 & 0 & \eta & 0 & \alpha_1 & 0 & -\delta_1 & 0 \\ 0 & 0 & 0 & 0 & 0 & 0 & 0 & \alpha_2 & -\delta_1 \end{pmatrix}$$

The Jacobian of $f=(f_1,f_2,f_3,f_4,f_5,f_6,f_7,f_8,f_9)^T$ evaluated around disease free equilibrium (E_o) denoted by $J(E_o)$ is given by

$$J(E_0)\beta^c=\begin{pmatrix} -(\mu_h+\psi) & 0 & \psi & -x_1\beta_2 & 0 & 0 & 0 & 0 & -x_1\beta_1\frac{k}{(k)^2} \\ 0 & -(\mu_h+\pi_h) & 0 & \beta_2(x_1+\varpi x_3) & 0 & 0 & 0 & 0 & \beta_1\frac{k}{(k)^2}(x_1+\varpi x_3) \\ \omega & 0 & -(\mu_h+\psi) & -\varpi x_3\beta_2 & 0 & 0 & 0 & 0 & -\varpi x_3\beta_1\frac{k}{(k)^2} \\ 0 & \pi_h & 0 & -(\mu_h+d+\gamma) & 0 & 0 & 0 & 0 & 0 \\ 0 & 0 & 0 & \gamma-\varepsilon x_5\beta_2 & -\mu_h & 0 & 0 & 0 & -\varepsilon x_5\beta_1\frac{k}{(k)^2} \\ 0 & 0 & 0 & 0 & 0 & r_v(1-\frac{2N_v}{L})-\lambda_v-\mu_v & r_v(1-\frac{2N_v}{L}) & -x_6\tau_1\frac{k_1}{(k_1)^2} & -x_6\tau_2\frac{k_2}{(k)^2} \\ 0 & 0 & 0 & 0 & 0 & \lambda_v & -\mu_v & -x_6\tau_1\frac{k_1}{(k_1)^2} & x_6\tau_2\frac{k_2}{(k)^2} \\ 0 & 0 & 0 & \eta & 0 & \alpha_1 & 0 & -\delta_1 & 0 \\ 0 & 0 & 0 & 0 & 0 & 0 & 0 & \alpha_2 & -\delta_1 \end{pmatrix}$$

The Jacobian $J(E_0)\beta^c$ of the linearized system has a simple zero eigenvalue (meaning that the remaining eigenvalues have negative real part). Hence, by center manifold theorem developed in (Castillo-Chavez et al., 2002), it is possible to analyze the dynamics of the system within $\beta_2=\beta^c$. Eigenvectors of $J(E_0)\beta^c$: Let $w=[w_1, w_2, w_3, w_6, w_8, w_9]^T$ and $v=[u_1, u_2, u_3, u_4, u_5, u_6, u_7, u_8, u_9]^T$ be the right and left eigenvectors, respectively, associated with the zero eigenvalue of the Jacobian of the linearized system $J(E0)\beta^c$, defined by:

$$w_1=\frac{a_3w_3}{\psi}>0,\quad w_2=\frac{\pi_hw_4}{a_2}>0,\quad w_3=\frac{\psi w_1}{a_3}>0,\quad w_4=\frac{a_4w_1+a_5w-a_6w_3+\eta w_8}{a_3}<0,$$

$$w_5=0,\quad w_6=\frac{\mu_vw_7}{a_{10}}>0,\quad w_7=0,\quad w_8=\frac{a_4w_1-a_5w_2+a_6w_3+a_7w_4-\gamma w_5}{\mu}>0,$$

$$w_9=-(\frac{\delta_1w_8+a_{11}w_6+a_{12}w_7}{a_2})<0, \tag{39}$$

And

$$u_1=\frac{-(a_3a_4+\psi a_6)u_4+(a_3a_{12}+\psi a_{14})u_9}{a_1a_3-\psi\omega}<0,\quad u_2=\frac{a_7u_4}{\pi_h}>0$$

$$u_3=\frac{-(\omega a_4+a_1a_6)u_4+(\omega a_{12}+a_1a_{14})u_9}{a_1a_3-\psi\omega}<0,\quad u_4=\frac{\pi_hu_2}{a_7}>0,\quad u_5=\frac{-\gamma u_4}{a_8}<0,$$

$$u_6 = \frac{-(a_{10}u_7 + a_{11}u_8 + a_{15}u_9)}{a_9} < 0, \qquad u_7 = \frac{a_{12}u_8 + a_{16}u_9}{\mu_v} > 0, \qquad u_8 = \frac{\delta_2 u_9}{\alpha_2} > 0$$

$$u_9 = \frac{\alpha_2 u_8}{\delta_2} > 0, \tag{40}$$

Following the Castillo-Chavez and Song theorem (Castillo-Chavez et al., 2002), we compute the associated backward bifurcation parameters A and B that are responsible for the direction of bifurcation,

$$A = \sum_{k,i,j=1}^{n} u_k w_i w_j \frac{\partial^2 f_k(0,0)}{\partial x_i \partial x_j}, \qquad B = \sum_{k,i,=1}^{n} u_k w_i \frac{\partial^2 f_k(0,0)}{\partial x_i \partial \beta^c}, \tag{41}$$

After computing the non-zero second order partial derivatives of f as defined in (3.16), and evaluating around diseases free E0, we obtain

$$\begin{aligned} A = {} & \frac{2\beta_1}{k^2}(S_h^0(u_1 w_9^2 - u_9^2) + \sigma V_h^0(u_3 w_9^2 - u_9^2)) + \frac{2\beta_1}{k}\left((u_2 - u_1)w_1 w_9 + \sigma(u_2 - u_3)w_3 w_9\right) \\ & + 2\beta_2\left((u_2 - u_1)w_1 w_4 + \sigma(u_2 - u_3)w_3 w_4\right) - 2\left(u_6 w_6^2 + u_7 w_6 w_7\right)\left(\tau_2 + \tfrac{\tau_1}{L_0}\right) \\ & + \frac{2}{k_1^2}\left(\tau_1 S_v^0 u_6 w_8 - \tfrac{\tau_1}{k_2} S_v^0 u_7 w_8\right) + \frac{2}{k_2^2}\left(\tau_2 S_v^0 u_6 w_8 - \tfrac{\tau_2}{k_1} S_v^0 u_7 w_9\right) + \frac{2u_7 w_8 \tau_1}{k_2} + \frac{2v_7 w_6 w_9 \tau_2}{k_1 k_2} \end{aligned} \tag{42}$$

And

$$B = \frac{w_9(u_2 - u_3)\sigma V_h^0 + (u_2 - u_1)S_h^0}{k} \tag{43}$$

which indicates that $B > 0$. Hence, backward bifurcation exists only if $A > 0$.

Theorem 5.2. The disease-free equilibrium E_0 of model (3) is globally asymptotically stable if $R_0 < 1$ and unstable if $R_0 > 1$.

The global stability is proved for a special case $\beta_2 = 0$ and $\epsilon = 0$. T hus, the modified model is given as

$$\begin{aligned} \frac{dS_h}{dt} &= \Lambda_h - \hat{\lambda}_h S_h - (\mu_h + \omega)S_h + \psi V_h \\ \frac{dE_h}{dt} &= \hat{\lambda}_h S_h + \sigma\hat{\lambda}_h V_h - (\mu_h + \pi_h)E_h \\ \frac{dV_h}{dt} &= \omega S_h - (\mu_h + \psi)V_h - \sigma\hat{\lambda}_h V_h \\ \frac{dI_h}{dt} &= \pi_h E_h - (\mu_h + d + \gamma)I_h \\ \frac{dR_h}{dt} &= \gamma I_h - \mu_h R_h \\ \frac{dS_v}{dt} &= r_v N_v\left(1 - \frac{N_v}{L}\right) - \lambda_v S_v - \mu_v S_v \\ \frac{dE_v}{dt} &= \lambda_v S_v - \mu_v E_v \\ \frac{dC}{dt} &= \eta I_h + \alpha_1 E_v - \delta_1 C \\ \frac{dP}{dt} &= \alpha_2 E_v - \delta_2 P \end{aligned} \tag{44}$$

Where

$$\hat{\lambda}_h = \frac{\beta_1}{k+P} \tag{45}$$

The associated reproduction number for model (51) is presented as:

$$\hat{R}_0 = \rho(FV^{-1}) = \frac{1}{2}\left(D + \sqrt{D^2 + 4BC}\right) \tag{46}$$

Proof. Following the approach of (Castillo-Chavez et al., 2002), let $X = (S_h, V_h, R_h, S_v)^T$ be non-infected classes and $Z = (E_h, I_h, E_v, C, P)^T$ be infected classes. Thus, our model can be written in the form

$$\frac{dX}{dt} = F(X,Z)$$

$$\frac{dZ}{dt} = G(X,Z)$$

Where

$$\begin{aligned} F(X,Z) &= (\Lambda_h - \hat{\lambda}_h S_h - (\mu_h + \omega)S_h + \psi V_h, \omega S_h - (\mu_h + \psi)V_h, \gamma I_h - \mu_h R_h \\ &\quad r_v N_v\left(1 - \frac{N_v}{L}\right) - \lambda_v S_v - \mu_v S_v) \\ G(X,Z) &= (\hat{\lambda}_h S_h + \sigma\hat{\lambda}_h V_h - (\mu_h + \pi_h)E_h, \pi_h E_h - (\mu_h + d + \gamma)I_h, \\ &\quad \lambda_v S_v - \mu_v E_v, \eta I_h + \alpha_1 E_v - \delta_1 C, \alpha_2 E_v - \delta_2 P) \end{aligned} \tag{47}$$

Condition (i). Set $Z = 0$ and consider the uninfected subsystem $\frac{dX}{dt} = F(X,0)$; we obtain

$$\begin{aligned} \frac{dS_h}{dt} &= \Lambda_h - \mu_h S_h \\ \frac{dV_h}{dt} &= \omega S_h - (\mu_h + \psi)V_h \\ \frac{dS_v}{dt} &= r_v N_v\left(1 - \frac{N_v}{L}\right) - \mu_h S_v \end{aligned} \tag{48}$$

Following (Castillo-Chavez et al., 2002), the disease-free equilibrium point E_0 is a globally asymptotically stable (G.A.S) equilibrium of (28) provided that $R_0 < 1$ if the following conditions are satisfied.

Condition i: For $\frac{dX}{dt} = F(X, 0)$, the equilibrium point X is globally asymptotically stable.

Condition ii: $\hat{G}(X, Z) = AZ - G(X, Z)$, where $\hat{G}(X, Z) \geq 0$ for all $X, Z \in \Omega$.

To show Condition i, we solve system (48) converges to their respective points in the DFE, E_0, as $t \to \infty$. The equation (48) can be obtained as

$$S_h(t) \to S_h^0 = \frac{\Lambda_h}{\mu_h}, \quad V_h(t) \to V_h^0(t) = \frac{\omega\Lambda_h}{\mu_h(\mu_h + \psi)}, \quad S_v(t) \to S_v^0(t) = L \tag{49}$$

Thus, the uninfected subsystem has a globally asymptotically stable equilibrium $(S_h^0, V_h^0, R_h^0, S_h^0)$

the biologically feasible region. Hence Condition (i) of the Castillo–Chavez framework (Castillo-Chavez et al., 2002) is satisfied.

Condition (ii). We write the infected subsystem in the form

$$\hat{G}(X,Z) = AZ - G(X,Z), \tag{50}$$

$$G(X,Z) = \begin{pmatrix} \hat{\lambda}_h S_h + \sigma\hat{\lambda}_h V_h - (\mu_h + \pi_h)E_h \\ \pi_h E_h - (\mu_h + d + \gamma)I_h \\ \lambda_v S_v - \mu_v E_v \\ \eta I_h + \alpha_1 E_v - \delta_1 C \\ \alpha_2 E_v - \delta_2 P \end{pmatrix} \tag{51}$$

$$A = \begin{pmatrix} -(\mu_h + \pi_h) & 0 & 0 & 0 & (S_h^0 + \sigma V_h^0)\frac{\beta_1}{k} \\ \pi_h & -(\mu_h + d + \gamma) & 0 & 0 & 0 \\ 0 & 0 & -\mu_v & S_v^0 \frac{\tau_1}{k_1} & S_v^0 \frac{\tau_2}{k_2} \\ 0 & \eta & \alpha_1 & -\delta_1 & 0 \\ 0 & 0 & \alpha_2 & 0 & \delta_2 \end{pmatrix} \tag{52}$$

$$\hat{G}(X,Z) = AZ - G(X,Z),$$

$$\hat{G}(X,Z) = \begin{pmatrix} (S_h^0 + \sigma V_h^0)\frac{\beta_1}{k}P - \hat{\lambda}_h S_h - \sigma\hat{\lambda}_h V_h \\ 0 \\ S_v^0 \frac{\tau_1}{k_1} C + S_h^0 \frac{\tau_2}{k_2} P - \hat{\lambda} S_v \\ 0 \\ 0 \\ 0 \end{pmatrix} \tag{53}$$

$$\hat{G}(X,Z) = \begin{pmatrix} (\frac{(S_h^0 - S_h)k + S_h^0 P}{k(k+P)})\beta P + (\frac{(V_h^0 - V_h)k + V_h^0 P}{k(k+P)})\sigma\beta_1 P \\ 0 \\ (\frac{(S_v^0 - S_v)k_1 + S_h^0 P}{k_1(k_1 + C)})\tau_1 C + (\frac{(S_v^0 - S_v)k_2 + S_v^0 P}{k_2(k_2 + P)})\tau_2 P \\ 0 \\ 0 \\ 0 \end{pmatrix} \tag{54}$$

Since $0 \le S_h(t) \le \frac{\Lambda_h}{\mu_h}, \quad 0 \le V_h(t) \le \frac{\omega\Lambda_h}{\mu_h(\mu_h + \psi)}$ and $0 \le S_v(t) \le L,$ then it follows that $\hat{G}(X,Z) \ge 0.$

Thus E_0 is GAS whenever $\hat{R}_0 < 1.$

Validation

The model was validated by comparing simulated results with observed cholera cases data obtained from Nigeria Centre for Disease Control (NCDC) between the period of 2022–2024. The model was compared based on the monthly reported cholera cases over three years, which is 36-month period (from January 2022 - December 2024),

as presented in Figure 2 and Table 1. The goodness of fit was assessed using Root Mean Square Error (RMSE) and the coefficient of determination (R^2).

$$RMSE = \sqrt{\frac{1}{n}\sum_{i=1}^{n}(y_i - \hat{y}_i)^2}$$

$$R^2 = 1 - \frac{\sum(y_i - \hat{y}_i)^2}{\sum(y_i - \bar{y})^2} \tag{55}$$

Figure 2 illustrates the comparison between observed data and estimated number of infected individuals predicted by the model (I_h) over time (monthly).

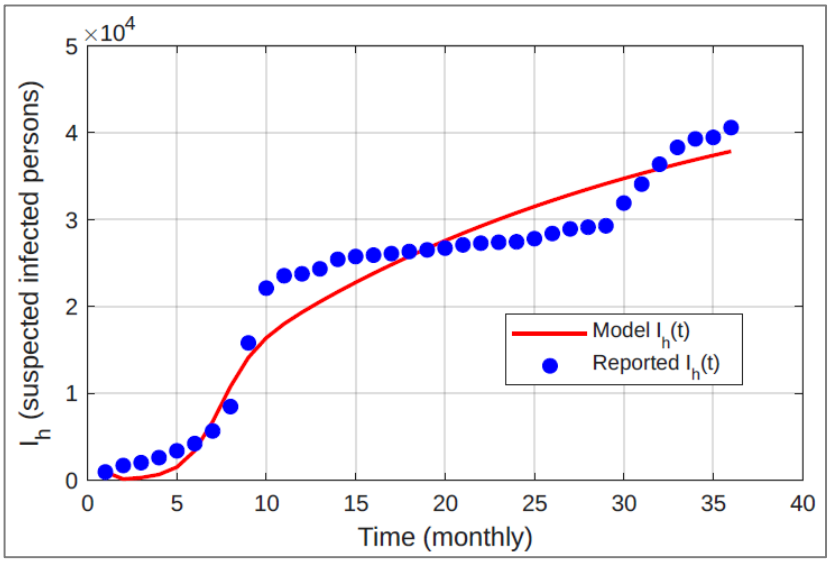

Figure 2: Observed data obtain from (NCDC) fitted with a model solution

Parameter Estimation

Table 1: Parameter Description and Values for Cholera Model.

Parameter	Description	value (Monthly)	Reference
Λ_h	Recruitment rate into human population	2500	Assumed
μ_h	Natural death rate of humans	0.0019	(Onuorah et al., 2022)
ω	Vaccination rate of susceptible humans	0.5642	Estimated
ψ	Waning rate of vaccine-induced immunity	0.8833	Estimated
π_h	Progression rate from E_h to I_h	0.0871	Estimated
d	Disease-induced death rate in humans	0.05	(Namawejje et a., 2018)
γ	Recovery rate of infected humans	0.2	(Hartley et al., 2006)
σ	Relative susceptibility of vaccinated individuals	1.0000	Estimated
ϵ	Reinfection rate	0.1474	Estimated
β_1	Human infection rate via environmental pathogen P	0.0007	Estimated
β_2	Human infection rate via contact with infected humans	0.0001	Estimated
k_1, k_2	Half-saturation constants for P and C	10^6	(Onuorah et al., 2022)
r_v	Intrinsic growth rate of vector population	0.03	Assumed
μ_v	Natural death rate of vectors	0.23	(Bertuzzo et al., 2011)
L	carrying capacity	2000	(Mukandavire et al., 2011)
τ_1	Vector infection rate via contaminated environment C	0.2116	Estimated
τ_2	Vector infection rate via environmental pathogen P	0.5458	Estimated
a_1	Shedding rate of bacteria into environment by vectors	0.02	(Modnak, 2017)
a_2	Shedding rate of bacteria into Food or water by vectors	0.03	(Modnak, 2017)
η	Contribution of I_h to environmental contamination	0.2180	Estimated
δ_1	Decay rate of bacteria in environment	0.01	(Isere et al., 2014)
δ_2	Decay rate of bacteria in Food or water	0.01	(Isere et al., 2014)

Model parameters were obtained from the published literature and, where necessary, estimated by fitting the model to available cholera case data. The fitting was performed using a least-squares approach to minimise the difference between the observed and simulated data. Some parameters were assumed due to limited data availability, but their influence on model outcomes was examined through sensitivity analysis. Table 1 presents the parameter description and values for the cholera model.

Sensitivity Analysis of the Model

In this section, Partial Rank Correlation Coefficient (PRCC) is used to study the sensitivity of the model output due to changes in some specific parameter values (Figure 3). The effective reproduction number R_0 is used as the response function for the PRCC. If a parameter falls on the positive side, then R_0 will increase as the parameter increases. However, if the sensitivity index of a parameter is negative, then R_0 decreases as the parameter increases. The results of the (PRCC) illustrate the degree of effect of each parameter that most strongly influences the basic reproduction number R_0 in the extended model of transmission of cholera. Generally, the PRCC analysis identifies the key parameters driving cholera transmission in the model. The strongest contributors to an increase in R_0 include Λ_h, β_2, τ_2, π_h, and L, while μ_h, μ_r, γ, and δ_2 are the most important parameters reducing R_0. This information is valuable for guiding targeted control strategies aimed at reducing disease spread.

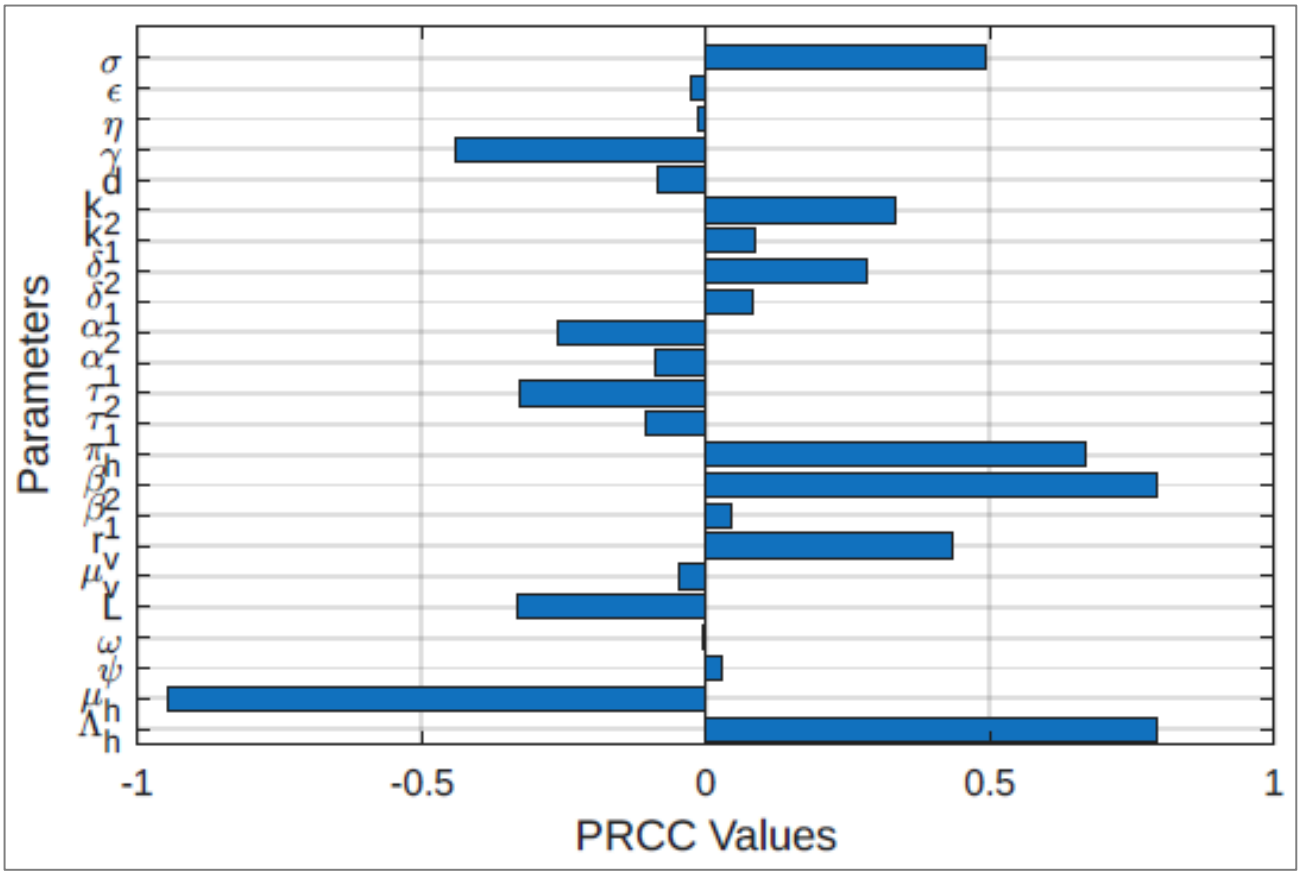

Figure 3: Parameters affecting reproduction number

Numerical Simulation

In this section, we perform a numerical simulation of the model system Equations (3) to demonstrate our simulation results and to illustrate the asymptotic behaviour of the model. The systems of differential equations were solved over a specific period of time period using Range- Kutta method embedded in MATLAB with ode45. The parameter values used in the simulations are given in Table 1

Effect of Re-infection

The above Figure 4, illustrates the dynamics of infected individuals over a period of 120 months under two scenarios, with and without re-infection. $\varepsilon = 0$ (Without re-infection): Recovered individuals acquire permanent immunity. Consequently, the number of infected individuals declines over time, leading to possible disease elimination. $\varepsilon \neq 0$ (With re-infection) Immunity wanes, and recovered individuals can be re-infected. This leads to a higher and more persistent number of infected individuals in the population. Re-infection enhances disease persistence and increases

the burden of cholera, emphasizing the importance of considering waning immunity in transmission modeling. These results indicate the critical role of re-infection in maintaining cholera endemic. Models that did not consider re-infection may underestimate the long-term disease burden, whereas incorporating re-infection provides more realistic description of cholera dynamics, particularly in regions where immunity is temporary. Consequently, sustained control strategies such as continuous vaccination, improved sanitation, and access to clean water are essential for effective disease management.

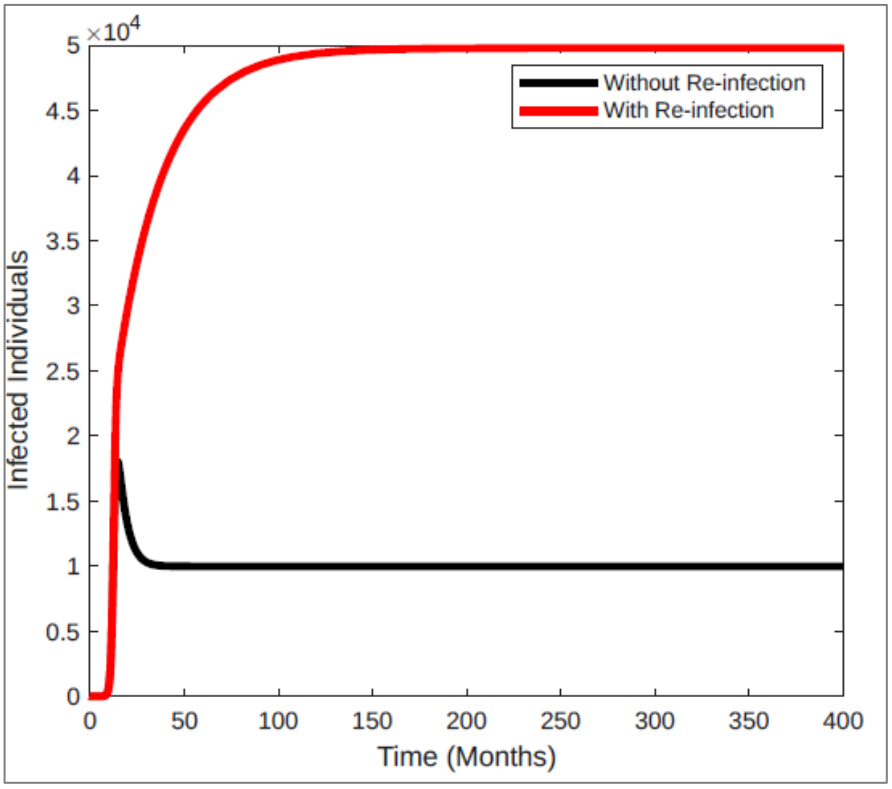

Figure 4: Infection Dynamic with and without Re-infection

Assessing the role of Vaccine with $\sigma = 0$

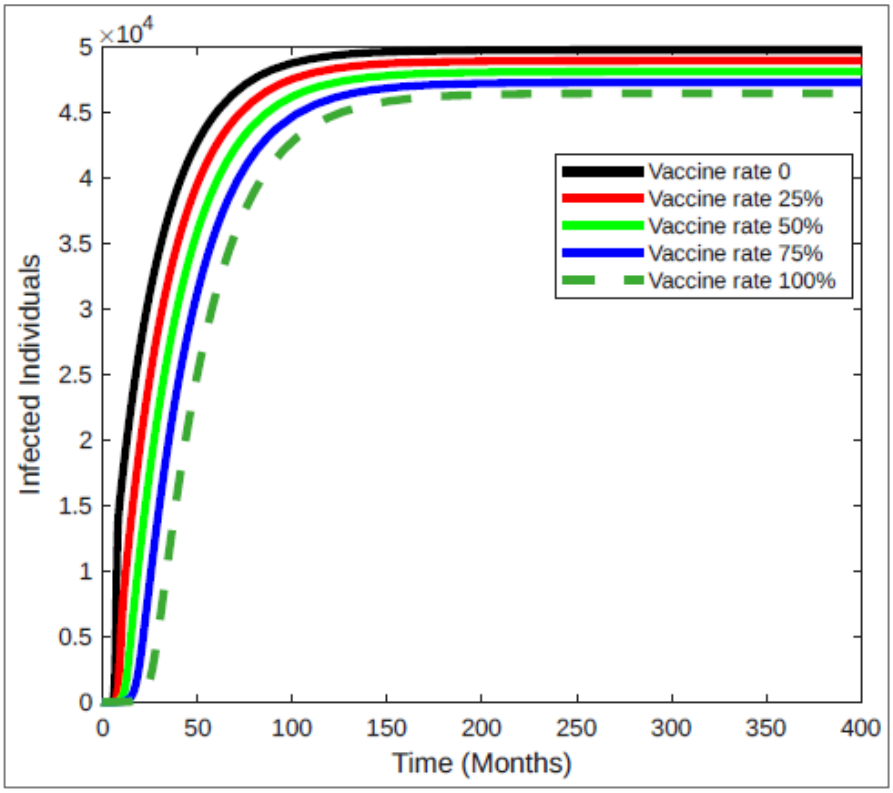

Figure 5: Vaccine with $\sigma = 0$

Figure 5 illustrates the effect of varying vaccination rates on the number of Vacinated individuals over time. In the absence of vaccination, the number of infected individuals increases rapidly and stabilizes at a high endemic level, indicating persistent disease transmission. As the vaccination rate increases to 25% and 50%, a noticeable reduction in the peak and endemic level of infections is observed, although the disease remains present in the population. At higher vaccination rates (75%), the infected population declines significantly, approaching disease elimination. When the vaccination rate reaches 100%, the number of infected individuals decreases to zero, indicating complete eradication of the disease. These results demonstrate that vaccination substantially reduces cholera transmission and that high vaccination coverage is essential for effective disease control and elimination.

Assessing the role of Vaccine with $\sigma \neq 0$

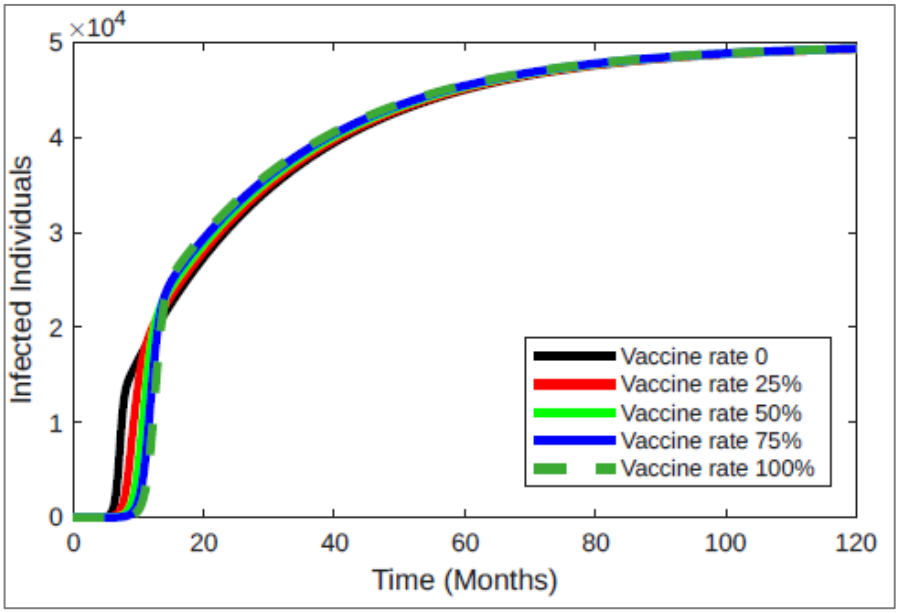

Figure 6: Vaccine with $\sigma \neq 0$

Figure 6 illustrates the dynamics of vaccinated individuals for different vaccination rates over time. When the vaccination rate is zero, the vaccinated population remains at zero throughout the simulation, showing the absence of vaccination. When the vaccination rate increases to 25% and 50%, the vaccinated population increases gradually and approaches higher steady-state levels. At higher vaccination rates (75% and 100%), the number of vaccinated individuals increases rapidly and stabilizes at significantly larger values. These results show that increasing vaccination coverage leads to a higher proportion of vaccinated individuals in the population, thereby reducing susceptibility to infection. This supports the effectiveness of vaccination as a key intervention strategy for controlling and eliminating cholera.

Vaccination Rate Density Plot

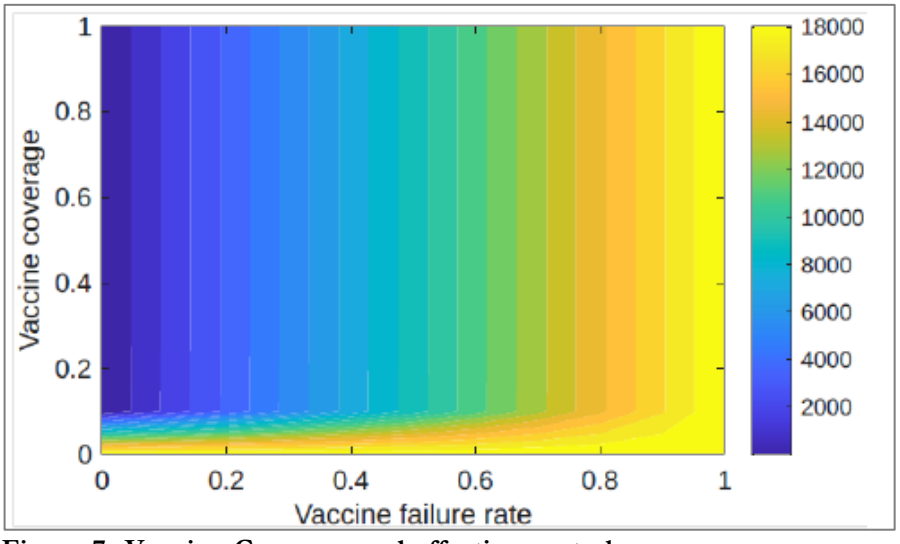

Figure 7: Vaccine Coverage and effective control

Figure 7 shows that the color bar indicate that darker blue color indicate to lower density levels, whereas brighter yellow colors indicate higher density levels. Figure 7 illustrates that vaccination is most effective when both vaccine coverage and vaccine effectiveness are high. As the vaccine failure rate increases, the disease burden rises sharply, even at high levels of vaccine coverage. In contrast, when the vaccine failure rate is low, increasing vaccine coverage leads to a substantial reduction in disease transmission. The highest disease levels occur when vaccine coverage is low, and the failure rate is high. Overall, the figure emphasizes that effective disease control depends not only on vaccinating a large proportion of the population but also on ensuring that the vaccine provides strong and reliable protection.

DISCUSSION

The research developed an extended deterministic compartmental model to investigate the transmission dynamics of cholera by incorporating three critical components: a vaccinated human popu-lation, an exposed human compartment, and vector recruitment, which was modelled using logistic growth, which contributes to environmental contamination. The human host is divided into five compartments: susceptible, vaccinated, exposed, infected, and recovered. The vector population is divided into two compartments: susceptible and exposed vectors. The environmental reservoir divides the environment into safe and unsafe environments according to the concentration of *Vibrio cholerae*. We established that the model is epidemiologically feasible and well-posed, and we also showed the existence of the disease-free equilibrium. Furthermore, we employed the next generation matrix technique to derive the reproduction number R_0. We proved that the model has two equilibrium points; the disease-free equilibrium, which is locally asymptotically stable whenever $R_0 < 1$, and unstable otherwise. We performed the sensitivity analysis on the reproductive number, R_0. Our analyses revealed that the parameter human recruitment rate Λ_h introduces more susceptible individuals into the population, thereby enhancing transmission potential. Similarly, the human-to-human transmission rate β_2, the high-level environmental shedding rate τ_2, and the progression rate from exposed to infectious individuals π_h exhibit strong positive correlations with R_0. Contrarily, the natural death rate of humans μ_h shows a strong negative correlation with R_0. Higher values of μ_h decrease the number of individuals available for infection, thereby lowering transmission. Other parameters with notable negative influence include the vector mortality rate μ_v, the human recovery rate γ, and the environmental pathogen decay rate δ_2. Numerical simulations were carried out to confirm the theoretical analysis and explore more patterns of dynamical behaviours of our model. The analytical results showed that the basic reproduction number depends on the combined influence of human-to-environment, human-to-human, and vector-mediated transmission pathways. The model demonstrates that increasing vaccination coverage and improving vaccine effectiveness reduce cholera transmission, but these measures alone may not guarantee disease elimination due to the persistence of environmental reservoirs and reinfection. Numerical simulations further confirmed that integrated intervention strategies, including vaccination, improved sanitation, vector control, and early treatment, are essential for achieving effective and sustainable cholera control.

CONCLUSION

The results of the model highlight the significant role of environmental contamination and vaccination in cholera transmission dynamics. The inclusion of an exposed compartment and vector logistic growth provides a more realistic disease progression compared to existing models.

The findings are consistent with previous studies based on SIRB and SEIR frameworks, which emphasize the importance of environmental reservoirs in sustaining cholera outbreaks.

However, the model has some limitations such as:

seasonal variations such as rainfall, temperature, and environmental conditions that influence cholera outbreaks. Seasonal effects can significantly affect both vector population dynamics and environmental contamination levels.

stochastic modeling approaches could be explored to account for random variations and un-certainties in disease transmission, particularly in small populations or during the early stages of an outbreak.

optimal control theory to determine the cost effectiveness intervention strategies, including vaccination, treatment, sanitation improvement, and vector control.

fractional-order differential equations to capture memory effects in disease transmission processes, which may provide a more accurate description of cholera dynamics.

Despite these limitations, the model provides useful insights into effective intervention strategies, particularly the combined use of vaccination and environmental sanitation.

REFERENCES

Al-Shanfari, S., ELmojtaba, I. M., & Alsalti, N. (2019). The role of houseflies in cholera transmission. *Communications in Mathematical Biology and Neuroscience*, Article 31. [Crossref]

Bertuzzo, E., Mari, L., Righetto, L., Gatto, M., Casagrandi, R., Blokesch, M., ... Rinaldo, A. (2011).

Prediction of the spatial evolution and effects of control measures for the unfolding Haiti cholera outbreak. *Geophysical Research Letters*, 38(6). [Crossref]

Castillo-Chavez, C., Feng, Z., & Huang, W. (2002). On the computation of R_0 and its role on global stability. In C. Castillo-Chavez, S. Blower, P. van den Driessche, & et al. (Eds.), *Mathematical approaches for emerging and reemerging infectious diseases: Models, methods and theory* (pp. 229-250). Springer. [Crossref]

CDC. (2019). *Cholera - Vibrio cholerae infection*. [Link]

CDC. (2021). *Premiumtimes*. [Link]

CDC. (2024). *NCDC*. [Link]

Das, P., Mukherjee, D., & Sarkar, A. K. (2005). Study of a carrier dependent infectious disease - cholera. *Journal of Biological Systems*, 13(2), 233-244. [Crossref]

Edward, S., & Nyerere, N. (2015). A mathematical model for the dynamics of cholera with control measures. *Applied and Computational Mathematics*, 4(2), 53-63. [Crossref]

Fister, K. R., Gaff, H., Lenhart, S., & Schaefer, E. (2016). Optimal control of vaccination in an age-structured cholera model. In G. Chowell & J. M. Hyman (Eds.), *Mathematical and statistical modeling for emerging and re-emerging infectious diseases* (pp. 221-248). Springer. [Crossref]

Fotedar, R., Banerjee, U., Samantray, J. C., & Shriniwas. (1992). Vector potential of hospital houseflies with special reference to *Klebsiella* species. *Epidemiology and Infection*, 109(1), 143-147.

Hai-Feng, H., & Na-Na, S. (2012). Global stability for a binge drinking model with two stages. *Discrete Dynamics in Nature and Society*, 1-15. [Crossref]

Harris, J. B., LaRocque, R. C., Kadri, F., Ryan, E. T., & Calderwood, S. B. (2012). Cholera. *The Lancet*, 379(9835), 2466-2476. [Crossref]

Hartley, D. M., Morris Jr., J. G., & Smith, D. L. (2006). Hyperinfectivity: A critical element in the ability of *V. cholerae* to cause epidemics? *PLoS Medicine*, 3(1), e7. [Crossref]

Hove-Musekwa, S. D., Nyabadza, F., Chiyaka, C., Das, P., Tripathi, A., & Mukandavire, Z. (2011). Modelling and analysis of the effects of malnutrition in the spread of cholera. *Mathematical and Computer Modelling*, 53(9-10), 1583-1595. [Crossref]

Isere, A., Osemwenkhae, J., & Okuonghae, D. (2014). Optimal control model for the outbreak of cholera in Nigeria. *African Journal of Mathematics and Computer Science Research*, 7(2), 24-30. [Crossref]

Ishaku, A., & Hussaini, N. (2020). Modelling effects of HCV plus-strand RNA influx into a cell during HCV replication. *Journal of the Indonesian Mathematical Society*, 26(1), 37-54. [Crossref]

Kaka, R., & Anteneh, L. M. (2024). Mathematical modelling and analysis of cholera dynamics via vector transmission. *Communications in Mathematical Biology and Neuroscience*, Article 74. [Crossref]

Keiding, J. (1986). *The house-fly: Biology and control* (Technical Report). World Health Organization.

Lata, K., Mishra, S. N., & Misra, A. K. (2020). An optimal control problem for carrier dependent diseases. *Biosystems*, 187, 104039. [Crossref]

Levine, O. S., & Levine, M. M. (1991). Houseflies (*Musca domestica*) as mechanical vectors of shigellosis. *Clinical Infectious Diseases*, 13(4), 688-696. [Crossref]

Misra, A. K., Mishra, S. N., Pathak, A. L., & et al. (2013). A mathematical model for the control of carrier-dependent infectious diseases with direct transmission and time delay. *Chaos, Solitons and Fractals*, 57, 41-53. [Crossref]

Modnak, C. (2017). A model of cholera transmission with hyperinfectivity and its optimal vaccination control. *International Journal of Biomathematics*, 10(6), 1750084. [Crossref]

Mukandavire, Z., Liao, S., Wang, J., Gaff, H., Smith, D. L., & Morris Jr., J. G. (2011). Estimating the reproductive numbers for the 2008-2009 cholera outbreaks in Zimbabwe. *Proceedings of the National Academy of Sciences*, 108(21), 8767-8772. [Crossref]

Namawejje, H., Obuya, E., & Luboobi, L. S. (2018). Modeling optimal control of cholera disease under the interventions of vaccination, treatment and education awareness. *Journal of Mathematics Research*, 10(5), 137-152. [Crossref]

Nelson, E. J., Harris, J. B., Morris, J. G., Calderwood, S. B., & Camilli, A. (2009). Cholera transmission: The host, pathogen and bacteriophage dynamic. *Nature Reviews Microbiology*, 7(10), 693-702. [Crossref]

Omondi, E. O. (2016). *A mathematical model for onchocerciasis and its treatment with ivermectin* [Master's thesis, University of Stellenbosch].

Onuorah, M. O., Atiku, F., & Juuko, H. (2022). Mathematical model for prevention and control of cholera transmission in a variable population. *Research in Mathematics*, 9(1), 2018779. [Crossref]

Pascual, M., Koelle, K., & Dobson, A. P. (2006). Hyperinfectivity in cholera: A new mechanism for an old epidemiological model? *PLoS Medicine*, 3(6), e280. [Crossref]

van den Driessche, P., & Watmough, J. (2002). Reproduction numbers and sub-threshold endemic equilibria for compartmental models of disease transmission. *Mathematical Biosciences*, 180(1-2), 29-48. [Crossref]

WHO. (2011). Weekly epidemiological record, 2011, vol. 86, 36 [full issue]. *Weekly Epidemiological Record*, 86(36), 389-400.

Yang, C., Wang, X., Gao, D., & Wang, J. (2017). Impact of awareness programs on cholera dynamics: Two modeling approaches. *Bulletin of Mathematical Biology*, 79, 2109-2131. [Crossref]